Simple theory of low-temperature thermal conductivity in single- and double-walled carbon nanotubes

D. V. Chalin, M. V. Avramenko, and S. B. Rochal
Department of Nanotechnology, Faculty of Physics, Southern Federal University, 5, Zorge Street, Rostov-on-Don 344090, Russia
(Received 7 June 2017; published 5 October 2017)

Low-temperature phonon thermal conductance (PTC) of any 1D system increases proportionally to the temperature. However, here we show that in single- and double-walled carbon nanotubes (CNTs), starting from 3–6 K, the PTC increases faster than the linear function, since the low-frequency modes of dispersion curves, which do not tend to zero together with the wave vector, are excited. To develop the PTC theory, we combine the Landauer's ballistic approach with the simple continuous model proposed for the calculation of the low-frequency phonon spectra of both free nanotubes and those interacting with an environment. The approach obtained is valid not only for commensurate double-walled CNTs, but also for incommensurate ones. The temperature-dependent relation between the PTC of double-walled CNT and those of its constituent SWNTs is obtained and discussed. The low-temperature heat transfer in bulk materials originated from CNTs is also considered and the upper limit of thermal conductivity of such materials is determined. We argue that the ideal material consisting of CNTs can challenge diamond only when the mean length of its defect-free nanotubes reaches at least one hundred of micrometers.

DOI: 10.1103/PhysRevB.96.155413

I. INTRODUCTION

Current progress in electronics and optoelectronics stimulates interest in investigation of thermal conductivity (TC) of different materials because the performance and stability of nanoelectronic devices are substantially determined by their cooling effectiveness. Due to a combination of unique electrical and thermal properties, carbon nanotubes (CNTs) and their different nanocomposites are considered to be the promising materials for development of the new-generation nanoelectronic devices [1,2]. However, despite the great number of both theoretical and experimental papers devoted to TC of CNTs and their nanocomposites, this topic is still a matter of intense debate.

The first experiment to estimate the TC coefficient of bulk samples (or "mats") of single-walled carbon nanotubes (SWCNTs) bundles was conducted in 1999: a dense-packed SWCNT mat had a room-temperature TC of 36 $\mathrm{W\,m^{-1}\,K^{-1}}$) [3]. Having corrected this value for the data on electrical conductivity of SWCNT bundles, the authors of Ref. [3] obtained the TC value of 1800−6000 $\mathrm{W\,m^{-1}\,K^{-1}}$ for a single rope of SWCNTs at room temperature. The measurements [3] were performed at $8 < T < 350$ K and the form of temperature dependence of TC coefficient was close to linear. One year later, a paper [4] devoted to measurements of TC coefficients in two thin films consisted of aligned SWCNT bundles at $10 < T < 400$ K emerged. A form of the dependence obtained was similar to the one published in Ref. [3], but the room-temperature value of the TC coefficient was about 200 $\mathrm{W\,m^{-1}\,K^{-1}}$. Later, TC coefficients of individual SWCNTs were measured at $110 < T < 800$ K [5–7], but the results presented in those papers were quite contradictory.

TC of SWCNTs and its dependence on temperature were also studied theoretically in several tens of papers [8–22]. It is almost generally accepted that in low-temperature range (at $T < 100$ K) the main contribution to TC of CNTs is made by phonons [8–21] and individual defectless CNTs are practically ideal heat conductors [23] due to the very large value of phonon mean free path l_f. According to the estimation of Ref. [24], l_f value in sufficiently long CNTs can be up to several tens of micrometers. At low temperatures, such l_f values are explained by two factors. First, in the 1D nanotubes, the mean concentration of phonons increases slower with temperature than in 2D or 3D systems [23]. Second, for the phonons, whose frequencies are determined by special dispersion relations, it is more difficult to satisfy energy and momentum conservation laws in the case of the lowest dimensionality [25–27].

So, in the low-temperature region (where the l_f value is large in comparison with a CNT length), the heat transfer can be described in the framework of ballistic (or Landauer's) mechanism [28,29], which implies that the phonons, moving freely along a CNT, are scattered only at its ends. However, with the temperature increase, this approximation becomes incorrect (the longer a CNT is, the sooner the mechanism stops working) and the TC becomes primarily of diffusion type [23], for which umklapp processes and phonon-phonon interactions are essential but difficult factors to account for. Certainly, this is the reason why known theoretical results predicting high-temperature TC of CNTs are contradictory. In particular, at $T = 300$ K, the theoretical TC of SWCNTs is reported to be from 29.8 to 10000 $\mathrm{W\,m^{-1}\,K^{-1}}$ [8–22].

It is also worth noting that the length of a SWCNT can just slightly exceed the l_f value at $100 < T < 300$ K and, consequently, a crossover from the ballistic regime to the diffusive one may take place. The thermal transport in such a "transitional" regime can be considered within the framework of the so-called quasiballistic approach [30], which allows one to avoid difficulties in taking phonon interactions into account and express the thermal conductance coefficient in terms of the nanotube length and the l_f value.

Nevertheless, some important unsolved problems still exist even in the low-temperature range, which is relatively simple for developing theoretical models. Despite the fact that the Landauer's ballistic approach was applied to investigate the phonon thermal conductance (PTC) of SWCNTs several times [24,31,32], the case of double-walled carbon nanotubes

(DWCNTs) still has not been studied well. Obviously, this fact can be associated with difficulties in the modeling of phonon spectra since many DWCNTs are incommensurate systems. Although the thermal conductivity of commensurate DWCNTs was studied in a number of papers [33–37] by means of molecular dynamics simulations, the results obtained by the authors of these articles cannot be directly or indirectly compared with the theory we propose. In Refs. [33–37] neither the results of thermal conductivity calculations in low-temperature range nor the phonon spectra of considered commensurate DWCNTs are presented.

In this paper, to develop the PTC theory, we combine the Landauer's ballistic approach with the simple continuous model proposed for the calculation of the low-frequency phonon spectra of both single- and double-walled CNTs. The use of continuous approach allows us to obtain simple analytical expressions for the frequencies of all the modes that mainly contribute to the resulting low-temperature PTCs.

The dependence of PTC on temperature is obtained for both individual nanotubes and those interacting with their environment. For free individual CNTs, all such dependencies tend to zero with $T \to 0$ and have the same slope in this point, which is explained by the specific quantum nature of PTC in 1D systems [31,32,38,39]. However, starting from 3–6 K [this temperature depends on the nanotube type and its diameter(s)], the PTC increases faster than the linear function, since the low-frequency modes of dispersion curves, which do not tend to zero together with the wave vector, are excited. Besides, we have revealed that a temperature T_0 about 15 K is very important for the characterization of PTC in DWCNTs. Studying and comparing the PTC of a DWCNT (PTC_D) with the thermal conductances of inner (PTC_i) and outer (PTC_o) uncoupled nanotubes (forming this DWCNT), we have obtained that if $T < T_0$ then the modes corresponding to the relative motion of the walls in DWCNT are frozen and, as a result, the following relation takes place: $PTC_i < PTC_D < PTC_o$. At temperatures higher than T_0, PTC_D exceeds both PTC_i and PTC_o but remains lower than their sum ($PTC_i + PTC_o$). These utterly unexpected relations are explained by the specific features found in the CNT dynamics.

Along with the theoretical investigation of ballistic PTC in CNTs of different types, here we propose the simplest model describing ballistic heat transfer in actively studied [40–45] CNT composite materials. The model allows us to estimate the upper possible values of TC in such composites and demonstrate that CNT composites cannot challenge synthetic diamond at 5 K $< T <$ 100 K until the mean length of CNTs in a composite material becomes at least one hundred of micrometers. The fact that at ultralow temperatures, the TC of CNTs increases with temperature faster ($\sim T$) than the one of diamond ($\sim T^3$) does not improve the situation either.

The paper is organized as follows. The classical theory of TC in one-dimensional systems (including individual CNTs) is revisited in the next section. Section III is devoted to the simplest theory describing low-frequency phonon modes in CNTs since only these modes are excited at low temperatures. At such excitations, neighboring atoms move with close phases, just as it occurs when sound propagates in ordinary crystals. Therefore, to calculate the frequencies of these "quasiacoustic" modes in CNTs (both individual and interacting with environment), we adapt and revise the continuous theory of phonon dynamics [46,47]. In Sec. IV, for SWCNTs and DWCNTs, we derive and discuss the PTC temperature dependencies in the frame of the continuous approach proposed. Finally, in Sec. V, we compare the developed theory with known experimental data and analyze future prospects of applying CNT composite materials as macroscopic thermal conductors. The paper ends with Conclusion.

II. BALLISTIC APPROACH TO THERMAL CONDUCTANCE OF CARBON NANOTUBES

It is commonly accepted that the model of low-temperature ballistic PTC originates in the pioneer papers of Landauer, who considered a one-dimensional conductive channel when studying the electrical conductance of metals. Assuming that the electron mean free path in such a channel is much greater than the channel's length, Landauer obtained his famous expression, which states that the electrical conductance value can be quantized [28,29]. Later, his ideas were advanced in Refs. [38,48] devoted to discussions of information flow in a one-dimensional channel [48] and phonon heat transfer in a quantum wire [38].

Let us note that the choice of the ballistic approach rather than the quasiballistic one [30] for further consideration is determined by the fact that the use of the latter is reasonable at temperatures higher than the temperature limit of any CNTs continuous dynamics theory (including the approach presented in Sec. III).

As is generally known [3], heat in CNTs is mainly transferred by phonons. Therefore let us consider the phonon PTC of an individual free nanotube in detail. If the latter is at constant temperature, then the heat flow transferred by phonons from its left end to the right one is equal to the heat flow transferred in the opposite direction. Let us denote the absolute value of these flows as j. Then

$$j = \frac{1}{2L}\sum_{s,k} \hbar\omega_s(k)\eta(\omega_s, T)\frac{\partial\omega_s(k)}{\partial k}\zeta_s(\omega), \qquad (1)$$

where k is a one-dimensional wave vector, $\omega_s(k)$ is the dispersion of a phonon mode with number s, $\partial\omega_s(k)/\partial k$ is the group velocity, and $\eta(\omega_s, T) = 1/[\exp(\frac{\hbar\omega_s(k)}{k_B T}) - 1]$ stands for the Bose-Einstein distribution. The function $\zeta_s(\omega)$ corresponds to the probability that a phonon with frequency ω of a mode s is transferred from the one end of a one-dimensional system to the other end without scattering [24,31,32,38,39,49]. In general, $0 \leqslant \zeta_s(\omega) \leqslant 1$, but ballistic mechanism of heat transfer by definition implies that $\zeta_s(\omega) = 1$.

Equation (1) is correct, in principle, for any one-dimensional phonon heat conductor, where phonons possess not only frequency but also wave vector. The total number of resulting dispersion curves $\omega_s(k)$ indexed by s depends on the internal structure of a considered nanotube. In Ref. [38], where a one-dimensional dielectric heat conductor was discussed, variable s changed from 1 to 3. In SWCNTs (as in ordinary crystals), the number of dispersion curves is three times greater than m, where m is a number of carbon atoms per one nanotube unit cell. Note that m is necessarily divisible by 4 [50].

It should be pointed out that there are some difficulties with application of Eq. (1) to DWCNTs. Two nanotubes, which form a DWCNT, are often incommensurate to each other. In this case, it is impossible to define a unit cell in such DWCNT and, consequently, the notion of wave vector [which is present in Eq. (1)] becomes unclear. However, for low-frequency "quasiacoustic" modes (when neighboring atoms move with close phases), the dynamics of DWCNT can be considered in a continuous approximation. Thus, at low frequencies, the wave vector notion is justified and Eq. (1) can be used at low temperatures.

After the remark made above we can proceed further. Let us assume that temperatures T_1 and T_2 are maintained at the left and right ends of the nanotube under consideration, respectively, and the value $\Delta T = T_1 - T_2$ is sufficiently small. Then the uncompensated heat flow Δj is expressed as

$$\Delta j = \frac{\partial j}{\partial T}\Delta T. \tag{2}$$

Substituting (1) into (2) and defining the PTC of a nanotube as $\kappa = \Delta j/\Delta T$, we get

$$\kappa = \frac{1}{2L}\sum_{s,k}\hbar\omega_s(k)\frac{\partial\omega_s(k)}{\partial k}\frac{\partial\eta(\omega_s,T)}{\partial T}\zeta_s(\omega). \tag{3}$$

Below, we start to utilize the ballistic approximation and simplify Eq. (3) assuming that $\zeta_s(\omega) = 1$. However, we do not use the total transmission function $\zeta(\omega) = \sum_s \zeta_s(\omega)$ [51], which is equal to the number of dispersion curves $\omega_s(k)$ crossing a line of constant frequency ω because, in our opinion, there is no point in using it in the frame of ballistic approach.

For a SWCNT, the conversion of the sum in Eq. (3) into a definite integral with respect to the wave vector k and then replacing this variable to proceed to the integration over frequency ω yields

$$\kappa = \frac{1}{2\pi}\sum_s\int_{\omega_s|_{k=0}}^{\omega_s|_{k=\frac{\pi}{a}}}\hbar\omega\frac{\partial\eta(\omega,T)}{\partial T}d\omega, \tag{4}$$

where a is a period of the considered SWCNT. Equation (4) clearly demonstrates that the thermal conductance of a SWCNT is determined only by the frequencies of the phonon modes in the center of the first Brillouin zone (FBZ) and on its boundaries [24,31,32,38,39]. A substitution of x for $\hbar\omega_s/k_BT$ in Eq. (4) allows us to get

$$\kappa = \frac{k_B^2T}{h}\sum_s\int_{x_{\min}(s,T)}^{x_{\max}(s,T)}\frac{x^2e^x}{(e^x-1)^2}dx, \tag{5}$$

where $x_{\min}(s,T) = (\frac{\hbar\omega_s}{k_BT})|_{k=0}$ and $x_{\max}(s,T) = (\frac{\hbar\omega_s}{k_BT})|_{k=\frac{\pi}{a}}$. At $T \to 0$, Eq. (5) tends to the constant value. To calculate it, let us note that for a dispersion curve, which has zero frequency in the center of the FBZ, $\lim_{T\to0} x_{\min} = 0$ and $\lim_{T\to0} x_{\max} = \infty$ and, consequently, the integral in Eq. (5) yields $\pi^2/3$. Thus each dispersion curve, which has zero frequency in the center of the FBZ, makes a fixed contribution $\kappa_0 = \pi^2k_B^2T/\,3h$ to the PTC of SWCNT. Analogously, if a dispersion curve has a nonzero frequency in the center of the FBZ, then its contribution to Eq. (5) tends to zero at $T \to 0$.

The quantization of PTC of a 1D system in the framework of the ballistic approach was proposed for the first time in Ref. [38] and later experimentally proven in Ref. [39]. It is notable that the value κ_0, which is the PTC quantum, is universal and does not depend on the type of statistics [38,52,53]. In addition, let us note that the energy of any individual free nanotube should be invariant with respect to four Goldstone's variables corresponding to 3 translational and 1 rotational (about the axis of a nanotube) degrees of freedom. Thus four dispersion curves of the phonon spectrum of any free nanotube are to have zero frequencies in the center of the FBZ, and the phonon PTC of any nanotube is to be equal to $\kappa = 4\kappa_0 = 4\pi^2k_B^2T/\,3h$ at $T \to 0$. This fact is well known both for CNTs and other one-dimensional heat conductors [31,32,38,39].

Nevertheless, in order to calculate the thermal conductance not only at $T \to 0$ but also in a wider temperature region where the ballistic approach is still applicable, one should take into account the contribution of other dispersion curves, which have small but nonzero frequencies in the center of the FBZ. That could be done quite easily for any nanotube, which could be considered in a continuous approach (its region of applicability is justified for CNTs in the next section). Indeed, in a "virtual" continuous one-dimensional system, the wave vector k is not limited by the FBZ and the frequencies of all the dispersion curves $\omega_s(k)$ tend to infinity when increasing the absolute value of k. Repeating the transition from Eq. (3) to Eq. (5) in the continuous case, one can easily ascertain that Eq. (5) preserves its form and the values of $x_{\max}(s,T)$ always tend to infinity (not only at $T \to 0$). The low-frequency dispersion curves of SWCNTs and DWCNTs and the calculation of reduced frequencies $x_{\min}(s,T)$ are considered in the next section.

III. LOW-FREQUENCY DYNAMICS OF SINGLE- AND DOUBLE-WALLED CARBON NANOTUBES INTERACTING WITH ENVIRONMENT

Graphene and SWCNTs represent 2D membranes of one-atom thickness and, consequently, it is incorrect to describe them within an ordinary elasticity theory, which is valid only for membranes of a finite thickness [54–58]. As far as we know, this drawback was overcome for the first time in Ref. [59], where a continuous approach was proposed in order to derive a free energy density g for a SWCNT. Later, in Refs. [46,47], the expression for g was rewritten in equivalent form:

$$g = \frac{\lambda}{2}(\varepsilon_{ii})^2 + \mu\varepsilon_{ij}^2 + 2K(\Delta H)^2, \tag{6}$$

which we use below. In Eq. (6), λ and μ are 2D analogs of the Lame coefficients, K is topological bending rigidity, $\Delta H = H - H_0$ with H and H_0 standing for nonequilibrium and equilibrium mean curvatures of the surface, and ε_{ij} is a 2D strain tensor, which depends on H_0 and the 3D displacement field $\boldsymbol{u} = (u_r, u_\varphi, u_z)$ of a cylindrical membrane [46]. Let us recall that the latter depends on an angle φ and a variable z, which measures the distance along the cylinder axis. Using standard equations of differential geometry, one can find that the cylinder's mean curvature deviation is linearized with

respect to the field $\boldsymbol{u}$ and its derivative is equal to

$$\Delta H = -\frac{\Delta_s u_r}{2R^2}, \tag{7}$$

where $\Delta_s = 1 + \partial_\varphi^2 + R^2\partial_z^2$ [46]. It is worth noting that Eq. (6) can result in the well-known linearized equations of motion of *a flat* membrane [60], provided the appropriate expressions for ΔH and ε_{ij} are used.

Linearized equations of motion for a cylindrical membrane (their solutions determine the dependences of the displacement field $\boldsymbol{u}$ on the coordinates and time) are obtained by variation of the functional

$$A_R[\boldsymbol{u}] = \int \left(g(\boldsymbol{u}) - \frac{\rho}{2}\dot{\boldsymbol{u}}^2\right) dS dt, \tag{8}$$

where t is time, dS is the membrane area element, and ρ is the surface mass density. To derive the motion equations, we substitute $dS = Rdzd\varphi$, ΔH, and ε_{ij} in Eq. (8) and calculate the variation. The resulting equations have the following form:

$$\begin{aligned}
\ddot{u}_r \rho R &= -(\lambda+2\mu)\left(\frac{u_r}{R} + \frac{\partial u_\varphi}{R\partial\varphi}\right) - \lambda\frac{\partial u_z}{\partial z} - \frac{K}{R^3}\Delta_s^2 u_r,\\
\ddot{u}_\varphi \rho R &= \frac{\lambda+2\mu}{R}\left(\frac{\partial u_r}{\partial\varphi} + \frac{\partial^2 u_\varphi}{\partial\varphi^2}\right) + (\lambda+\mu)\frac{\partial^2 u_z}{\partial\varphi\partial z} + \mu R\frac{\partial^2 u_z}{\partial z^2},\\
\ddot{u}_z \rho R &= (\lambda+\mu)\frac{\partial^2 u_\varphi}{\partial\varphi\partial z} + (\lambda+2\mu)R\frac{\partial^2 u_z}{\partial z^2} + \lambda\frac{\partial u_r}{dz} + \mu\frac{\partial^2 u_z}{R\partial\varphi^2}.
\end{aligned} \tag{9}$$

In order to solve system (9), one should substitute $u_j = u_j^0 \exp[i(kz + n\varphi - \omega t)]$ in it, where $j = r, \varphi, z$, n is an integer wave number, k is a one-dimensional wave vector, and ω stands for circular frequency. Vanishing of the determinant of the obtained dynamic matrix

$$\boldsymbol{M}(R) = \begin{pmatrix}
\frac{\lambda+2\mu}{R} + \frac{KX^2}{R^3} - R\rho\omega^2 & i\frac{(\lambda+2\mu)n}{R} & ik\lambda \\
-i\frac{(\lambda+2\mu)n}{R} & \frac{(\lambda+2\mu)n^2}{R} + \mu k^2 R - R\rho\omega^2 & (\lambda+\mu)nk \\
-ik\lambda & (\lambda+\mu)nk & (\lambda+2\mu)k^2R + \frac{\mu n^2}{R} - R\rho\omega^2
\end{pmatrix}, \tag{10}$$

where $X = R^2k^2 + n^2 - 1$, determines three real dispersion laws $\omega_j = \omega_j(k,n)$. The imaginary values of nondiagonal blocks in (10) reflect the $\pi/2$ phase shift between the radial and tangential components of the displacement field.

The approximation of free nanotubes described above is quite rough. In a number of modern experiments, carbon nanotubes are located in a bundle or elastic medium. Thus the environment makes a contribution to the forces restoring nanotubes to their equilibrium state when thermal vibrations are excited. For individual nanotubes comprising any system, Goldstone degrees of freedom disappear since the system prevents free motion of nanotubes and, consequently, the frequencies of all nanotubes' modes cannot vanish at $k \to 0$. However, if a nanotube moves as a whole, then the elastic forces, resisting the longitudinal translation and rotation around the tube's axis, are significantly smaller than the forces resisting the radial motion [47]. Therefore only the latter forces are taken into account below: a simple pinning term $\frac{C}{2}u_r^2$ is added to the density of free energy (6). In this additional term, C stands for a coefficient, which describes the value of interaction between a nanotube and its environment. This additive also causes slight changes in Eqs. (9) and (10). Namely, the terms $-CRu_r$ and CR appear in the right part of the first equation of the system (9) and in M_{11} element of the dynamic matrix (10), respectively. Let us note that the value of C depends on the material of a CNT's environment and consequently could be different for various systems.

As we have shown above, in the framework of the continuous approach, the thermal conductance of CNTs is expressed in terms of the frequencies of the phonon modes with $k = 0$ only. At this value of the wave vector, the dynamic matrix $\boldsymbol{M}$ becomes quasidiagonal and the frequencies $\omega_1(n)$ of stretching and $\omega_2(n)$ of bending modes ($\omega_1 > \omega_2$) are obtained for every n value by solving the following quadratic equation in ω^2:

$$\begin{aligned}
\omega^4 - \left[\frac{\eta(n^2+1)}{\rho R^2} + \frac{K(n^2-1)^2}{\rho R^4} + \frac{C}{\rho}\right]\omega^2 \\
+ \frac{\eta n^2}{\rho R^2}\left[\frac{C}{\rho} + \frac{K(n^2-1)^2}{\rho R^4}\right] = 0,
\end{aligned} \tag{11}$$

where $\eta = \lambda + 2\mu$, and the frequency of the shear mode is

$$\omega_3(n) = \sqrt{\frac{\mu}{\rho}}\frac{n}{R}. \tag{12}$$

Correspondingly, the thermal conductance of a SWCNT in the framework of the continuous approach is expressed as

$$\kappa = \frac{k_B^2 T}{h}\sum_{n=-n_{\max}}^{n=n_{\max}}\sum_{i=1}^{3}\int_{x_{\min}(n,i,T)}^{\infty}\frac{x^2e^x}{(e^x-1)^2}dx, \tag{13}$$

where $x_{\min}(n,i,T) = (\frac{\hbar\omega_i(n,k)}{k_BT})|_{k=0}$ and $n_{\max}$ is derived from the expressions that determine the limits of applicability of the continuous model and are discussed below.

SWCNT phonons, which are indexed by n and k values, can be characterized by the effective wave vector

$$k_{\text{eff}} = \sqrt{k^2 + \left(\frac{n}{R}\right)^2}. \tag{14}$$

The continuous approach is applicable to SWCNTs provided the effective wavelength $2\pi/k_{\text{eff}}$ is several times longer than the interatomic distance $a_{C-C} = 0.142\,\text{nm}$. Thus we assume that the continuous model works for all modes, whose k_{eff} values are smaller than the limiting value of $k_{\text{eff}}^{\text{lim}} \approx 11\,\text{nm}^{-1}$. The latter estimation is easily obtained if the

effective wavelength $2\pi/k_{\text{eff}}$ is taken to be four times longer than a_{C-C}.

Equation (14) shows that the continuous approach is correct for the modes with $k = 0$ if the mode index n satisfies the condition $|n| \leqslant n_{\max}$, where $n_{\max} = Rk_{\text{eff}}^{\lim}$. It is clear that the maximal frequency $\omega_i^{\max}(n,k)$, corresponding to the limits of applicability of the continuous approach, exists for each dispersion curve with index $|n| \leqslant n_{\max}$ and wave number $k = k_{\max}(n)$ satisfying Eq. (14). Therefore the error of calculation of PTC by means of Eq. (13) is correlated with the fact that the frequencies $\omega_i^{\max}(n,k)$ do not tend to infinity and are equal to finite values. The latter component of the error under consideration is estimated as follows:

$$\Delta\kappa = \frac{k_B^2 T}{h} \sum_{n=-n_{\max}}^{n=n_{\max}} \sum_{i=1}^{3} \int_{x_{\max}(n,i,T)}^{\infty} \frac{x^2 e^x}{(e^x-1)^2} dx, \qquad (15)$$

where $x_{\max}(n,i,T) = (\frac{\hbar\omega_i^{\max}(n,k)}{k_B T})|_{k=k_{\max}}$. Thus the temperature region of applicability of the continuous approach to the ballistic PTC calculation is limited by the condition $\Delta\kappa \ll \kappa$.

Let us end the discussion of limitations of the continuous model with the following remark. The lengths of wave vector k (at which the continuous approach still works) can exceed the FBZ boundary of a particular SWCNT. It can then be translated back to the FBZ by adding the corresponding translations vectors of SWCNT's reciprocal space. Thus the dispersion curves of a SWCNT fold similarly to the case of phase transitions when the unit cell of the crystal is multiplied. When the dispersion curves are folded, some gaps (which are small in the region of the continuous approach applicability) can appear at the FBZ boundary. The small splitting of the dispersion curves at the FBZ boundary can also lead to a small additional error in the PTC calculation.

Now we proceed to DWCNTs, which can be also considered in the framework of the suggested continuous model. According to Refs. [46,61], the van der Waals interaction between two coaxial nanotubes forming the DWCNT has three simple components:

$$U_j = \frac{G_j}{2} \int \left(u_j^{(1)} - u_j^{(2)}\right)^2 d\varphi dz, \quad j = r,\varphi,z, \qquad (16)$$

where U_r, U_φ, and U_z are the contributions made by the radial, tangential transverse, and tangential longitudinal interactions; G_r, G_φ, and G_z are the material constants describing these interactions; $u_j^{(1)}$ and $u_j^{(2)}$ are the corresponding components of the displacement fields of the inner and outer nanotubes forming the DWCNT.

For the coupled cylindrical membranes, the equations of motion are obtained by variation of the following functional:

$$A[\boldsymbol{u}^{(1)},\boldsymbol{u}^{(2)}] = A_{R_1}[\boldsymbol{u}^{(1)}] + A_{R_2}[\boldsymbol{u}^{(2)}] + \int (U_r + U_\varphi + U_z) dt, \qquad (17)$$

where $A_{R_i}[\boldsymbol{u}^{(i)}]$ are two functionals with the form (8); R_1 and R_2 are the radii of the inner and outer nanotubes, respectively; $\boldsymbol{u}^{(i)}$ are the displacement fields of these nanotubes; t stands for time, and ρ is the surface mass density, which is identical for both nanotubes. The variation of functional (17) leads to a system of six equations which correspond to the components $u_j^{(1)}$ and $u_j^{(2)}$, where $j = r,\varphi,z$. Let us note that the set of three equations for the displacement field $\boldsymbol{u}^{(1)}$ is similar to the one for the field $\boldsymbol{u}^{(2)}$. The difference between these sets and the system (9) (which describes the single nanotube) is that the terms $G_j(u_j^{(1)} - u_j^{(2)})$ and $G_j(u_j^{(2)} - u_j^{(1)})$ are added to the sets for the outer and inner coupled nanotubes, respectively.

Substituting $u_j^{(\alpha)} = A_j^{(\alpha)} e^{i(kz+n\varphi-\omega t)}$, where $j = r,\varphi,z$ and $\alpha = 1,2$, in the resulting equations of motion, we derive the dynamic matrix $\boldsymbol{D}$ in the following form:

$$\boldsymbol{D} = \begin{pmatrix} \boldsymbol{M}(R_1) + \boldsymbol{E} & -\boldsymbol{E} \\ -\boldsymbol{E} & \boldsymbol{M}(R_2) + \boldsymbol{E} \end{pmatrix}, \qquad (18)$$

where the $\boldsymbol{M}(R_1)$ and $\boldsymbol{M}(R_2)$ blocks are obtained from the matrix (10) by replacing radius R with R_i; the matrix $\boldsymbol{E}$ is diagonal and its elements are equal to the constants G_r, G_φ, and G_z. The vanishing of the determinant of the dynamic matrix (18) specifies six real dispersion laws: $\omega_j = \omega_j(k,n)$.

Let us note that the low-frequency phonon spectrum of a DWCNT substantially differs from the simple superposition of the phonon spectra of the two SWCNTs comprising it. This is due to the fact that four $\boldsymbol{E}$ blocks, which are equal to each other and take into account van der Waals interactions between DWCNT's layers, appear in the dynamic matrix (18). The addition of the diagonal $\boldsymbol{E}$ blocks to $\boldsymbol{M}(R_1)$ and $\boldsymbol{M}(R_2)$ slightly increases the eigenfrequencies of the both SWCNTs. In particular, this effect is the main reason why the frequencies of breathinglike modes in a DWCNT are higher than the ones of radial breathing modes in individual SWCNTs comprising a DWCNT [46]. At the same time, if the antidiagonal - $\boldsymbol{E}$ blocks were absent, then there would be no dispersion curves tending to zero frequency at $k \to 0$ and, in fact, the phonon spectrum of a DWCNT would resemble a superposition of the spectra of two uncoupled SWCNTs being in a quasielastic medium. Let us stress that the presence of these blocks (taking into account the interaction between coaxial CNTs) in the matrix (18) leads to the substantial difference between the DWCNT's spectrum and the superposition of the spectra of two individual SWCNTs. In particular, the interlayer interaction results in the fact that the mode corresponding to the relative motion of inner and outer SWCNTs normal to the nanotubes' mutual axis (when the mass center is preserved) stops being of a Goldstone's type, and this relative motion of two nanotubes leads to appearance of the restoring force. For the same reason, the frequency of this doubly degenerate mode cannot be equal to zero at $k = 0$. In the same way, the frequencies of the modes corresponding to the relative rotation and slipping of two SWCNTs are not equal to zero at $k = 0$ either, because interlayer van der Waals interaction leads to the appearance of the tangential restoring forces. Thus, after a "virtual" formation of a DWCNT from individual SWCNTs, only four dispersion curves (out of eight) preserve zero frequencies at $k = 0$. Consequently, at $T \to 0$, the PTC of any free DWCNT is the same as the PTC of any free SWCNT.

The environmental influence on a DWCNT could be taken into account similarly to the case of a SWCNT—by adding the term $C R_2 (u_r^{(2)})^2/2$ to the free energy density $g(\boldsymbol{u}_2)$ of the outer nanotube. Thus one should obtain the corresponding changes

in the equation of motion for $u_r^{(2)}$ and the dynamic matrix (18):

$$\boldsymbol{D} \rightarrow \boldsymbol{D}' = \begin{pmatrix} \boldsymbol{M}(R_1) + \boldsymbol{E} & -\boldsymbol{E} \\ -\boldsymbol{E} & \boldsymbol{M}(R_2) + \boldsymbol{E}' \end{pmatrix}, \quad (19)$$

where the matrix $\boldsymbol{E}'$ differs from $\boldsymbol{E}$ only by one element, $E'_{11} = G_r + CR_2$.

At $k = 0$, the matrices (18) and (19) become quasidiagonal [as the matrix (10)] and split into 2D and 4D blocks. However, the resulting analytical equations for phonon frequencies are too cumbersome to present them here. Note also that the Eqs. (13) and (15) should be slightly changed to calculate the PTC of DWCNTs and estimate the error of the continuous approach. The only difference between the cases of DWCNTs and SWCNTs is that in the modified equations one should sum over the six phonon modes for every n. A more detailed application of the results obtained above to calculation of CNT thermal conductance is given in the next section.

IV. NUMERICAL ESTIMATIONS AND DISCUSSION OF CNT THERMAL CONDUCTANCE

In order to use the continuous model described in Sec. III, one should know the values of the material constants λ, μ, and K. Taking the values of sound velocity in graphene $v_{iLA} \approx 21.3\,\mathrm{km/s}$, $v_{iTA} \approx 13.6\,\mathrm{km/s}$ [62] and an estimation $K \approx 2.1\,\mathrm{Ev}$ [63] along with the known formulae $v_{iLA} = \sqrt{(\lambda + 2\mu)/\rho}$, $v_{iTA} = \sqrt{\mu/\rho}$ [46] we obtain the reduced material constants $\lambda/\rho \approx 2400\,\mathrm{cm^{-2}\,nm^2}$, $\mu/\rho \approx 5200\,\mathrm{cm^{-2}\,nm^2}$, $K/\rho \approx 12{,}5\,\mathrm{cm^{-2}\,nm^4}$, where $\rho \approx 0.762\,\mathrm{mg/m^2}$. The chosen system of units enables us to measure a CNT's diameter in nanometers and the frequency of modes in $\mathrm{cm^{-1}}$. Certainly, when a graphene sheet is rolled up into a carbon nanotube and, as a result, the surface acquires finite curvature radius, these material constants could be slightly changed in comparison with the ones of graphene. Nevertheless, due to the fact that the relation between the frequency of SWCNT's radial breathing mode and its diameter (which is easily derived in the framework of the continuous approach) scarcely depends on the nanotube chirality, we assume the material constants of graphene and carbon nanotubes to be equal to each other. Let us note that the chiral vector of SWCNTs (which determines the type of their electrical conductance) influences mainly the high-frequency part of CNT vibrational spectrum [50,64,65], originating from the optical modes of graphene. These modes are not described by the model under consideration.

Now let us digress to make an important remark about the free energy density of 2D membranes described in the framework of the continuous approach. The relation between the change of the mean curvature and the bending energy of a 2D membrane [the last term in Eq. (6)] was presented much earlier than in Ref. [59]. The first references date back to 1970s [66,67]. Later an alternative and more cumbersome relation for the free-energy density of a cylindrical membrane was proposed [68]: it included not only the term proportional to the squared mean curvature change but also the ones proportional to the product of ΔH and the diagonal components of the 2D strain tensor. From the symmetrical point of view, such terms are acceptable in the expression for the free energy density of a cylindrical membrane because they satisfy the translational and rotational invariance conditions. However, using the values of the reduced material constants, we have found that the dispersion curves obtained by solving the equation $\det|\boldsymbol{M}| = 0$ [see matrix (10)] and by means of the model [68] coincide within 1% provided the curves are compared in the limits of the continuous approach applicability. Thus there is no point in applying the more complicated model [68] in the present work.

A. Thermal conductance of an individual free SWCNT

The known material constants λ, μ, and K and the explicit forms of Eqs. (13)–(15) allow us to estimate the temperature limits of applicability of the continuous model for the calculation of SWCNT thermal conductance. Supposing $\Delta\kappa/\kappa < 0.01$ and assuming that the typical SWCNT radius is greater than 0.6 nm, but less than 1.5 nm, we obtain the applicability region of the model up to 75 K. Let us also note that the value $\Delta\kappa$ (15) does not directly determine the error of PTC calculation. Due to approximations discussed in the previous section, the relative error of PTC calculation may be several times higher than the value $\Delta\kappa/\kappa$. Let us also remark that the applicability region of the continuous approach depends on CNT radius, because the more the radius is, the more the $n_{\max}$ value becomes [see Eqs. (14) and (15)]. However, the contribution to $\Delta\kappa$ from the dispersion curves with large values of n is small, and our estimations show that the temperature dependence of the model's applicability limit is very weak.

Let us note that for the material constants found above, the following relation takes place:

$$\eta = \lambda + 2\mu \gg \frac{K}{R^2}. \quad (20)$$

Therefore, in addition, assuming that $\eta \gg CR^2$, one can solve Eq. (11) approximately, but with a good accuracy. For SWCNTs, the approximate frequencies $\omega_1(n)$ and $\omega_2(n)$, the stretching and bending modes, respectively, are

$$\omega_1(n) \approx \left[\frac{\lambda + 2\mu}{\rho R^2}(n^2 + 1) + \left(\frac{\omega_2(n)}{n}\right)^2\right]^{\frac{1}{2}}, \quad (21)$$

$$\omega_2(n) \approx \frac{n}{\sqrt{n^2 + 1}}\left[\frac{K(n^2 - 1)^2}{\rho R^4} + \frac{C}{\rho}\right]^{\frac{1}{2}}. \quad (22)$$

Equations (21) and (22) allow us to relate simply the cylindrical geometry with the flat one. In order to do it, we introduce an effective wave vector $q = n/R$ and neglect the small contribution of $\omega_2(n)$ to $\omega_1(n)$. Furthermore, it is seen that at $n \rightarrow \infty$ and $C = 0$, Eqs. (21) and (22) turn into the well-known dispersion laws for the longitudinal acoustic and bending modes of planar graphene: $\omega_1(n) = \sqrt{\eta/\rho}\,q$, $\omega_2(n) = \sqrt{K/\rho}q^2$.

Equation (22) determines the frequencies (at $k = 0$) of the lowest frequency bending modes, which make the most significant contribution to the ballistic PTC of SWCNTs. Figure 1 depicts the PTC dependencies on temperature for two free SWCNTs, which are of 0.61 and 1.5 nm in radius.

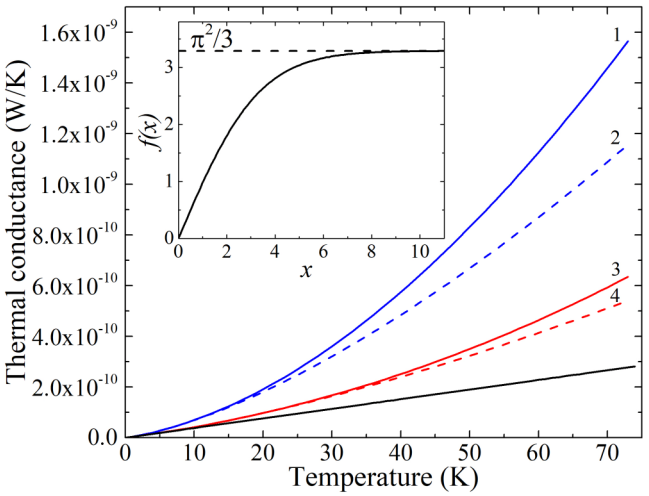

FIG. 1. Thermal conductance of individual SWCNTs (9, 9) and (26, 18). Curves with numbers 1 and 2 correspond to the nanotube with the larger radius, curves with numbers 3 and 4 to the one with smaller radius. Black line demonstrates the common low-temperature linear limit of thermal conductance of individual free nanotubes. The curves denoted with solid lines are obtained in terms of Eqs. (11)–(13). On the contrary, the curves denoted with dashed lines are calculated by means of approximate Eq. (23). The inset shows the function $f(x) = \int_0^x \frac{t^2 e^t dt}{(e^t-1)^2}$.

The first SWCNT could have (9, 9) indices and the second one (26, 18). At the lowest temperatures, only the modes of the dispersion curves, which tend to zero frequency at $k = 0$, are excited and the phonon PTC (being independent on SWCNT radius) is expressed as $\kappa = 4\kappa_0 = 4\pi^2 k_B^2 T/3h$ [31,32,38,39]. Along with the temperature rise up to 3–6 K, the lowest-energy bending modes with frequencies (22) and $n \geqslant 2$ are excited and PTC grows faster than the linear function. Let us note that the more CNT's radius is, the faster the PTC grows with temperature.

It is also interesting that within the temperature limit of the continuous approach applicability, the most significant contribution to the ballistic PTC is made by the acoustic and bending modes: it is about 80% for a SWCNT of 1 nm in radius even at $T \sim 73$ K. Thus, in order to estimate the thermal conductance of a SWCNT, we can use the following simple expression:

$$\kappa = 2\frac{k_B^2 T}{h}\sum_{n=0}^{n_{\max}}\int_{\frac{\hbar\omega_2(n)}{k_B T}}^{\infty}\frac{x^2 e^x}{(e^x-1)^2}dx, \qquad (23)$$

where frequencies $\omega_2(n)$ are determined by Eq. (22). Note that for a free nanotube ($C = 0$) the terms with $n = 0$ and $n = 1$ make the conventional contribution $4\kappa_0$ to Eq. (23).

Let us note that Eq. (23) turns out to be quite accurate: for a SWCNT of 1.5 nm in radius at $T < 11$ K the PTC values obtained using the approximate Eq. (23) and in terms of Eqs. (11)–(13) agree within 1% (see Fig. 1). For SWCNTs of smaller radii, the temperature region where the error is no more than 1% broadens and reaches the temperature of 30 K for a SWCNT of 0.61 nm in radius.

B. Thermal conductance of an individual free DWCNT

In order to consider the thermal conductance of an individual free DWCNT, we need to know the values of the coefficients describing the van der Waals interaction between its layers. One can estimate the value of G_r using the known relation [46] between the frequencies of breathinglike modes of DWCNTs and radial breathing modes of individual SWCNTs. Let us note that G_r slightly depends on the radii of the inner and outer nanotubes comprising a double-walled one. For the DWCNTs considered in Ref. [46], $1890 \leqslant G_r/\rho \leqslant 4010\,\mathrm{cm}^{-2}\,\mathrm{nm}$, while $0.8 \leqslant R_1 \leqslant 1.23$ nm (where R_1 stands for the inner radius of a DWCNT). The values of the material constants G_φ and G_z can be estimated only indirectly, using the graphite elastic moduli [61]. It is justified by the fact that the distance between graphite layers approximately equals to the interlayer one in DWCNTs. This approach cannot allow us to distinguish between the constants G_φ and G_z, thus we assume their values to be equal to each other (even though the symmetry of a DWCNT implies their difference). As a result, the following relations between G_r, G_φ, and G_z could be obtained:

$$\frac{G_r}{G_\varphi} \approx \frac{G_r}{G_z} \approx \frac{v_{\mathrm{LA}}^2}{v_{\mathrm{TA}}^2} \approx 7.75, \qquad (24)$$

where v_{LA} and v_{TA} are the velocities of the longitudinal and transversal acoustic modes of graphite, respectively.

Using the values of all material constants, one can estimate the temperature limit of the model applicability to the DWCNT case. For typical DWCNTs, $0.6 \leqslant R_1 \leqslant 1.8$, $0.9 \leqslant R_2 \leqslant 2.2$ nm, and the calculation, performed similarly to SWCNTs, limits the model by a temperature about 54 K.

We have calculated the PTC temperature dependence for the DWCNT (22, 14) at (40, 1) ($R_1 = 1.23$ nm, $R_2 = 1.58$ nm) as an example. The values of G_r for this nanotube were taken from Ref. [69], $G_r/\rho \approx 3850\,\mathrm{cm}^{-2}\,\mathrm{nm}$, after that, G_φ and G_z were obtained in terms of Eq. (24): $G_\varphi/\rho = G_z/\rho \approx 500\,\mathrm{cm}^{-2}\,\mathrm{nm}$. Solving the equation $\det|\boldsymbol{D}| = 0$ numerically at $k = 0$ and $C = 0$ and using the generalization of Eq. (13) for the case of a DWCNT (summation is to be over i from 1 to 6), one can easily obtain the plots presented in Fig. 2.

Note that the temperature T_0, which is about 15 K, is very special for the plots demonstrating PTC of DWCNTs. Comparing the thermal conductance of the DWCNT (22, 14) at (40, 1) ($\mathrm{PTC_D}$) with those of the inner ($\mathrm{PTC_i}$) and outer ($\mathrm{PTC_o}$) uncoupled nanotubes (forming this DWCNT), one can see that if $T < T_0$ (which is about 14 K in the case), then $\mathrm{PTC_i} < \mathrm{PTC_D} < \mathrm{PTC_o}$, else $\mathrm{PTC_D}$ exceeds both $\mathrm{PTC_i}$ and $\mathrm{PTC_o}$ but remains lower than their sum $\mathrm{PTC_i} + \mathrm{PTC_o}$ (see Fig. 2). This behavior is typical of DWCNTs and it is explained by the peculiarities of their low-frequency spectrum, which is determined by the equation $\det|\boldsymbol{D}| = 0$.

Let us consider this spectrum in more details. As we have already mentioned above, the secular equation $\det|\boldsymbol{D}| = 0$ splits at $k = 0$ into the ones of second and fourth orders. Analyzing the finite solutions of the latter equation at $\eta \to \infty$ and taking into account that $G_r \gg K/{R_1}^3$, one can easily obtain the approximate expressions $\omega_l(n)$ and $\omega_h(n)$ for the lowest frequency bending-like and composite (relative

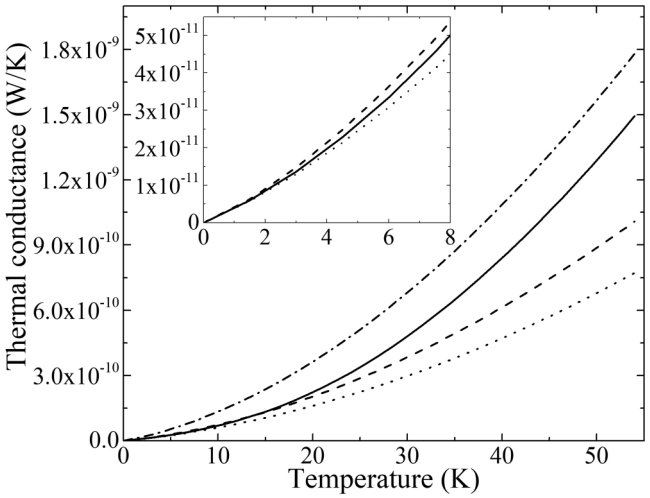

FIG. 2. Comparison of thermal conductance of the free DWCNT (22, 14) at (40, 1) and individual SWCNTs comprising it. Dashed and dotted lines demonstrate thermal conductances of the outer and inner nanotubes, respectively. Solid lines correspond to the thermal conductance of the individual DWCNT. Dash-dotted line demonstrates the sum of thermal conductances of individual SWCNTs. The inset shows the same curves on a larger scale.

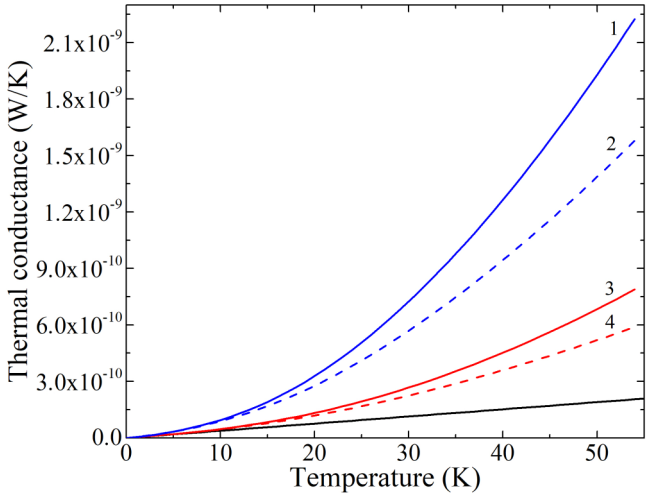

FIG. 3. Thermal conductance of individual DWCNTs (15, 1) at (19, 8) and (29, 25) at (42, 22). Curves 1 and 2 correspond to the nanotube with larger radii, while curves 3 and 4 to the nanotube with smaller ones. Black line demonstrates the common low-temperature linear limit for all individual free nanotubes. The curves denoted with solid lines are obtained in frames of the ballistic approach using the phonon spectrum calculated from the secular equation $\det|\boldsymbol{D}| = 0$. On the contrary, the curves denoted with dashed lines are obtained by means of approximate Eq. (27).

shear-bending) modes, which play a key role in the ballistic PTC of DWCNTs:

$$\omega_l(n) \approx \frac{n}{\sqrt{(n^2+1)(R_1+R_2)}} \times \left[\frac{K(n^2-1)^2}{\rho}\left(\frac{1}{R_1^3}+\frac{1}{R_2^3}\right)+\frac{CR_2}{\rho}\right]^{1/2}, \quad (25)$$

$$\omega_h(n) \approx \left\{\left(\frac{1}{R_1}+\frac{1}{R_2}\right)\frac{G_r n^2+G_\varphi}{\rho(n^2+1)}+\frac{1}{R_1+R_2}\frac{n^2}{n^2+1} \times \left[\frac{K(n^2-1)^2}{\rho}\left(\frac{R_2}{R_1^4}+\frac{R_1}{R_2^4}\right)+\frac{CR_1}{\rho}\right]\right\}^{\frac{1}{2}}, \quad (26)$$

where $\omega_l(n) < \omega_h(n)$ and $k = 0$. It is interesting that the expression $\omega_h(0)$ *exactly* determines the frequency of the mode corresponding to the relative rotation of inner and outer nanotubes. Since in our minimal model $G_\varphi = G_z$, $\omega_h(0)$ also coincides with the frequency of relative slipping of inner and outer nanotubes. Besides, note that Eq. (26) yields good accuracy provided $\eta \gg \frac{G_r n^2}{(n^2+1)^2} R_1$. Therefore the maximal error in $\omega_h(n)$ is found at $n = 1$, e. g., for the DWCNT (22, 14) at (40, 1), the relative error is about 9%. At $n \geqslant 2$, the accuracy of Eqs. (24) and (25) significantly increases until the condition $G_r \gg Kn^4/{R_1}^3$ is satisfied.

Equations (25) and (26) allow us to understand why $\mathrm{PTC_i} < \mathrm{PTC_D} < \mathrm{PTC_o}$ at $T < T_0$. Let us introduce an effective radius of a DWCNT, which is given by $R_{\mathrm{eff}} = [(R_1+R_2)R_1^3R_2^3/(R_1^3+R_2^3)]^{1/4}$, and, consequently, $R_1 < R_{\mathrm{eff}} < R_2$. After the substitution of R_{eff} into Eq. (25), the latter equation and Eq. (22) obtain an identical form provided $C = 0$. Thus T_0 is the temperature where the modes with frequencies (26) are not exited and the thermal conductance of a DWCNT is equivalent to that of a SWCNT with the effective radius R_{eff}. At $T > T_0$, the higher frequency part of a DWCNT's vibrational spectrum is excited and $\mathrm{PTC_D}$ starts to exceed both $\mathrm{PTC_i}$ and $\mathrm{PTC_o}$. In the light of all these considerations, one can estimate the low-temperature PTC of a DWCNT using the following approximate expression:

$$\kappa = 2\frac{k_B^2 T}{h}\sum_{n=0}^{n_{\max}}\sum_{\alpha=l,h}\int_{\frac{\hbar\omega_\alpha(n)}{k_B T}}^{\infty}\frac{x^2 e^x}{(e^x-1)^2}dx, \quad (27)$$

where the frequencies $\omega_\alpha(n)$ are calculated using Eqs. (25) and (26).

Thus the approximate Eq. (27) takes into account only the contribution of the lowest frequency bendinglike and composite modes. To analyze the quality of such approximation, we have chosen two DWCNTs, which are (15, 1) at (19, 8) with $R_1 = 0.61$ nm, $R_2 = 0.94$ nm, and (29, 25) at (42, 22) with $R_1 = 1.83$ nm, $R_2 = 2.2$ nm. According to Ref. [46], the G_r/ρ moduli for these nanotubes are about 3150 and 3630 cm^{-2} nm, respectively. For each of these DWCNTs, we have computed two plots: the first one is obtained by means of Eq. (27) and the second calculation uses the direct numerical solution of the secular equation. For the thicker DWCNT at $T < 10$ K, both plots agree within 1% accuracy (see Fig. 3). In turn, for the DWCNT of smaller radius, the temperature region of that accuracy broadens up to 15 K. For both DWCNTs even at $T = 54$ K, which is the temperature limit of the continuous model applicability, Eq. (27) yields more than 70% to the total PTC of both DWCNTs.

As it has been already stated in Introduction, the phonon spectra of commensurate DWCNTs may be calculated more precisely beyond the framework of continuous theory. Nevertheless, as far as we know, there is only one paper

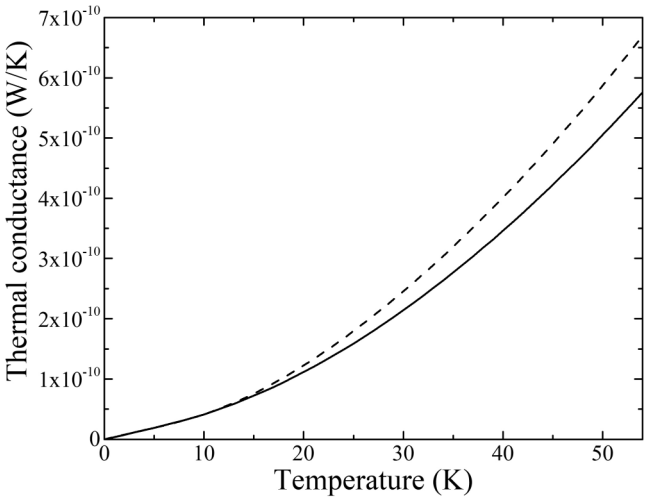

FIG. 4. Thermal conductance of an individual DWCNT (5, 5) at (10, 10) obtained within the framework of our model (solid line) and calculated on the basis of the phonon spectrum presented in the paper by M. Damnjanovic *et al.* [70] (dashed line).

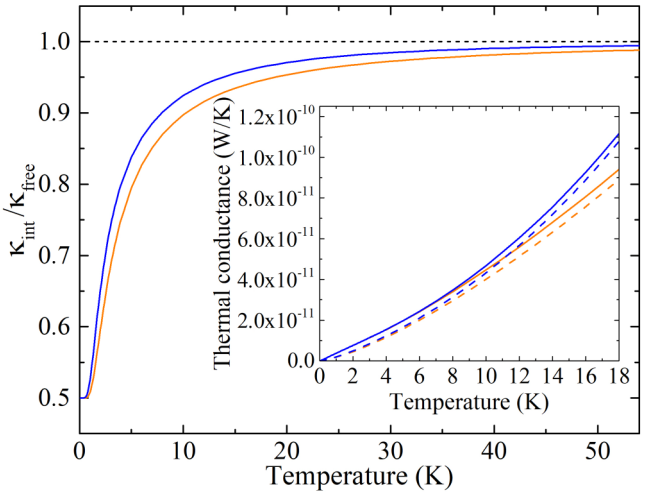

FIG. 5. The ratio $\kappa_{\rm int}/\kappa_{\rm free}$ of the thermal conductance of a pinned CNT and that of a free one. Curve 1 shows the temperature dependence of this ratio for the DWCNT (15, 1) at (19, 8), while the curve 2 does it for the SWCNT (18, 1). The inset shows the temperature dependencies of PTC for the chosen CNTs. Solid curves correspond to the free nanotubes; the dashed lines were obtained provided that the interaction between CNTs and their environment was taken into account ($C/\rho = 50\,\mathrm{cm}^{-2}$).

[70], where such calculations are performed analytically. In this article, devoted to symmetry and peculiarities of commensurate DWCNTs dynamics, a phonon spectrum of an individual DWCNT (5, 5) at (10, 10) obtained within the framework of the force-constant model is presented. In order to verify our model, we have calculated the ballistic thermal conductance of the same DWCNT and compared the obtained results with ours (see Fig. 4). As it can be seen, the thermal conductance calculated on the basis of the phonon spectrum [70] increases with temperature slightly faster that is due to some difference in frequencies of the spectra obtained within the approaches compared.

In our opinion, such difference in the spectra is mainly explained by the fact that the value of "effective" bending rigidity of the nanotube (which greatly depends on the choice of fitting parameters used in force-constant model [70]) turns out to be a bit less than the value we have taken from the more recent Ref. [63]. Owing to the smaller value of effective bending rigidity in Ref. [70], some phonon dispersion curves lower their frequencies. For instance, at $k = 0$ frequency, the difference can reach the value of several tens of cm^{-1} for some modes with wavenumbers, which do not exceed their upper limit in the continuous model. Consequently, the thermal conductance calculated on the basis of the phonon spectrum presented in the paper by M. Damnjanovic *et al.* [70] increases with temperature slightly faster.

It is also worth noting that in Ref. [70] the doubly degenerate transverse acoustic mode has a linear dispersion, although, as it is generally accepted, this mode is to have a quadratic one, according to the pioneer work in Ref. [71]. Thus the paper by M. Damnjanovic *et al.* [70] possibly needs sufficient revision, which, in our opinion, is beyond the scope of the present work. It is probable that a comparison of our theory with a more precise force-constant model of commensurate DWCNT dynamics could lead to a better match of both predicted phonon spectra and the physical properties of DWCNTs determined by them.

C. Environmental influence on thermal conductance

Now we return to the fact that in the majority of experiments, CNTs do interact with their environment and, therefore, cannot be considered as free ones. The radial pinning introduced previously in our model leads to the halving of PTC of any CNT at $T \to 0$, because the CNT pinned in a such way loses half of its Goldstone degrees of freedom. At the same time, the weak radial pinning barely influences the frequencies of the experimentally observed modes of SWCNTs and DWCNTs. In particular, at $C/\rho < 500\,\mathrm{cm}^{-2}$, the shift of the radial breathing mode of a SWCNT is less than the experimentally measurable instrumental error, namely $1\,\mathrm{cm}^{-1}$ [47].

However, the introduced pinning strongly affects the frequencies of bending modes of SWCNTs [see Eq. (22)], since at small n the values $\frac{Kn^4}{R^4}$ and C turn out to be of the same order of smallness. Nevertheless, the contribution of any phonon mode to PTC is determined not only by its frequency but rather by the temperature-dependent value $x_{\rm min} = \frac{\hbar\omega_i}{k_B T}$ [see Eqs. (11) and (12)]. Thus, if we discuss the experimentally considered temperature region starting at 8–10 K, then the weak environmental influence is not crucial. At sufficiently high temperatures $T > T_c$, a correction to $x_{\rm min}$ caused by pinning turns out to be small and T_c can be estimated as

$$T_c^2 \gg \frac{C\hbar^2}{\rho k_B^2}. \tag{28}$$

A similar consideration is also applicable to DWCNTs with the only difference that the right part of Eq. (28) is multiplied by $\frac{R_2}{R_1+R_2}$ and, consequently, the temperature region, where pinning should be taken into account, narrows. Our conclusions are illustrated in Fig. 5, where the environmental influence on the PTC of the SWCNT (18, 1) and the DWCNT

(15, 1) at (19, 8) is shown. Note that the radius of the former nanotube is equal to the effective radius of the latter one.

V. COMPOSITE MATERIALS WITH CNTs AS HEAT CONDUCTORS

All experimental studies of individual carbon nanotubes are quite difficult and most of TC measurements are carried out on samples consisting of SWCNT ropes or bundles. So, to compare predictions of the developed theory with the known experimental results, we have to relate the PTC of individual CNT with the TC of a bulk material containing CNTs. We solve this problem in the simplest way and consider a hypothetic composite material representing a heat insulator matrix containing heat conducting CNTs with a volume concentration c. Let the CNTs be arbitrarily oriented and have a mean length L. The concentration c is supposed to be small, thus the nanotubes are freely distributed throughout the composite and their different orientations are equally probable. Following the results of Ref. [45], we further simplify the model and assume that the thermal conductance between the ends of CNTs is infinite. Let a considered sample of composite material have the length H and the cross-sectional area S. Then the probability that an arbitrary chosen nanotube crosses the section S is expressed as

$$P = \frac{L\cos\theta}{H}. \tag{29}$$

If there is a certain temperature gradient grad$T$ between the ends of the bulk sample, a temperature difference between the ends of any nanotube is given by

$$\Delta T = L\cos\theta \,\mathrm{grad}T, \tag{30}$$

where θ is the angle between the nanotube orientation and the direction of grad$T$. Thus a total heat flow J across the section S is calculated as an average over all possible nanotubes orientations:

$$J = \langle HScP\Delta j\rangle. \tag{31}$$

Taking into account that the mean value of $\cos^2\theta$ over the sphere equals $1/3$, we obtain the following expression for the TC χ of the considered hypothetical composite:

$$\chi = \frac{cL^2}{3}\langle k\rangle. \tag{32}$$

where $\langle k\rangle$ is the mean thermal conductance of a single CNT.

Figure 6 shows the comparison of our results with the experimental data [3]. Using Eq. (32), we have fitted the experimental TC [3] of the sample containing SWCNT bundles. The average nanotubes' length and radius were taken from the same Ref. [3]. The best fitting of experimental data is achieved at $c \approx 2.49\times10^6\,\mu\mathrm{m}^{-3}$ and $C/\rho \approx 100\,\mathrm{cm}^{-2}$.

In conclusion of this paper, we will also consider the prospect of applying the CNT-based composite materials as bulk heat conductors. For this purpose, let us estimate the highest possible TC of such material. Recall that Eq. (32) was obtained in the limit of small nanotube concentration. In the opposite case of the maximal concentration (which corresponds to the maximal TC of the material), all nanotubes should be parallel to each other and CNT concentration in the matrix turns out to be inversely proportional to the mean volume occupied with one nanotube. Thus the TC coefficient becomes proportional to the average nanotube length L and its explicit form reads

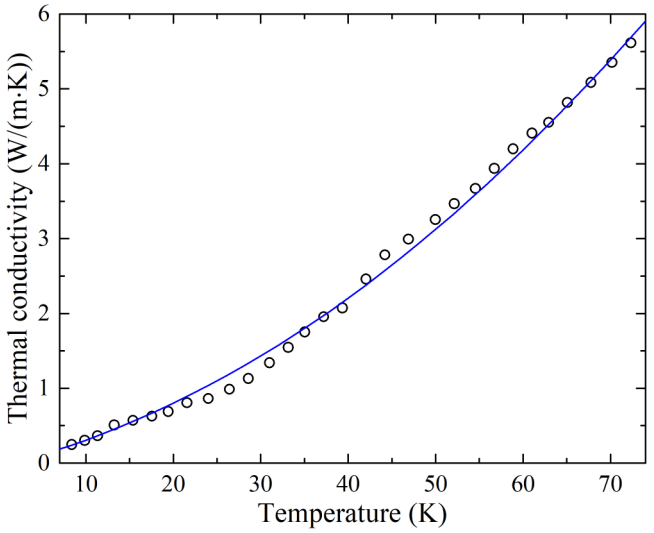

FIG. 6. Experimental thermal conductivity [3] (empty circles) of a sample containing SWCNT bundles; SWCNTs in the sample studied in Ref. [3] had a mean length of 100 nm and a mean diameter of 1.4 nm. The data fit (solid curve) was performed using Eq. (32).

$$\chi = \frac{2\sqrt{3}L}{3R_a^2}\langle\kappa\rangle, \tag{33}$$

where R_a is a mean distance between the nanotube axes in the perfect composite. Using Eq. (33), one can easily obtain the upper possible value for the TC of the hypothetical perfect composite material, in which the heat transfer is carried out by CNTs only. Note that the TC coefficient $\langle\kappa\rangle$ is a slowly increasing function of the CNT radius. Since the denominator of Eq. (33) contains R_a^2, then the highest value of TC coefficient χ is reached in composite materials consisting of CNTs with the minimal possible radii. Also, since TC of any DWCNT exceeds that of a SWCNT with the same radius at $T > 15$ K, it seems to be more effective to use DWCNTs instead of SWCNTs when designing the most perfect composite material. However, our further calculations demonstrate that the advantage of DWCNT usage is very small.

We calculated the TC temperature dependencies for two virtual ideal composite materials consisting of single- and double- walled carbon nanotubes with minimal possible radii (see Fig. 7). Since the mean length of CNTs is ordinarily of the order of few micrometers, in our calculations it is assumed to be 10 μm. In order to obtain the TC upper limit, the interaction between individual nanotubes in the composite is neglected ($C/\rho = 0\,\mathrm{cm}^{-2}$). As our estimations show, in spite of the nearly linear dependence of the composite TC on temperature, the diamond TC (which increases proportionally to T^3 at low temperatures) starts to exceed the latter one at temperatures of 5–7 K (see inset in Fig. 7). Slightly going beyond the limits of applicability of the continuous approach, here we extrapolate the curves describing the TC of ideal composites up to 100 K. It turns out that the obtained values of ideal composite's TC at

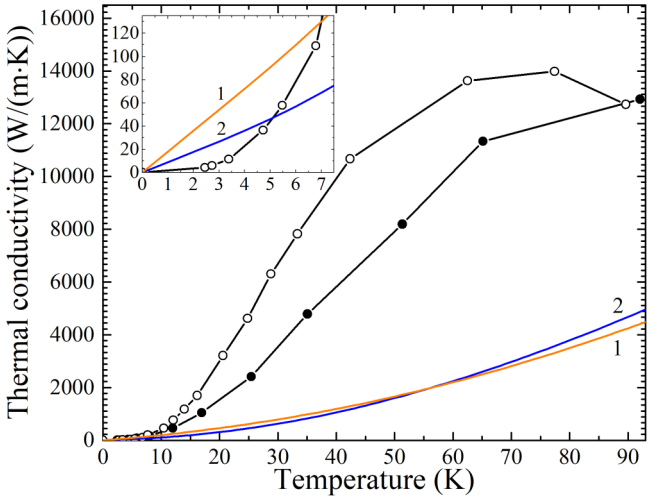

FIG. 7. Comparison of the thermal conductivities of diamond and the virtual perfect composite materials consisting of carbon nanotubes. TC plots of synthetic and natural (2a type) diamond [72,73] are denoted with filled and empty circles, respectively. Curves 1 and 2 are the TC temperature dependencies for two ideal composite materials (for more details see the text) consisting of SWCNTs (9, 9) and DWCNTs (15, 1) at (19, 8), respectively. In both composites the mean length of CNTs is chosen to be equal to 10 μm. The inset shows the thermal conductivities of the materials listed above at $T < 8$ K on a larger scale. Different outer radii of single- and double-walled carbon nanotubes used in the composites considered result in different slopes of curves 1 and 2 at $T \to 0$ [see Eq. (33)].

$T = 100$ K are an order of magnitude less than the TC of both synthetic and natural diamonds [72,73], whereas they are of the same order as the TC of pyrolytic graphite [74]. Moreover, according to our estimations, the unusually high values of the TC coefficient at $T = 100$ K, which were reported in a number of papers [9,11,14,22], could be implemented only in long CNTs with a phonon mean free path $l_f > 50\,\mu$m.

Certainly, we can also consider the longer nanotubes. Since Eq. (33) strongly depends on the nanotube mean length L, increase in this value leads to a proportional rise of the calculated TC. Nevertheless, it is obvious that to challenge the diamond, the real composite material (in contrast to the ideal one) should be based on defect-free nanotubes with the mean length exceeding at least one hundred of micrometers. Possibly, future progress in CNT synthesis will make the production and application of bulk materials based on CNTs of such length a reality. However, at present it seems more effective to use for heat exchange not bulk CNT composites but individual nanotubes, which can be successfully used in different nanodevices.

VI. CONCLUSION

In this paper, we develop the theory of low-temperature PTC of single- and double-walled CNTs. For this purpose, we use the Landauer's ballistic approach together with the proposed model of continuous dynamics. It allows us to calculate the low-frequency modes of phonon spectrum in both free CNTs and the ones interacting with their environment. At $T < 75$ K (this condition limits the region of joint applicability of continuous theory and ballistic approach for SWCNTs), the major contribution to the PTC of such nanotubes is made by low-frequency acoustic and bending modes. Furthermore, in the proposed framework, one can also consider DWCNTs, but only up to a temperature of about 55 K. In this case, a significant contribution to the PTC of a DWCNT is made not only by the acoustic and bending modes, but also by those corresponding to the relative rotation and slipping of two shells of the DWCNT.

It is well known that in the temperature region near the absolute zero, the PTC of free CNTs grows proportionally to the temperature increase. However, as we have shown, this temperature region is very small and starting from 3–6 K the PTC grows faster due to the consecutive excitation of the numerous low-frequency modes of CNTs. We have also obtained simple and previously unknown analytical expressions for frequencies of these modes, as well as the ones describing the PTC nonlinear dependence on temperature.

Considering the low-temperature PTC of free individual SWCNTs and DWCNTs, we have established the relation $\mathrm{PTC_i} < \mathrm{PTC_D} < \mathrm{PTC_o}$ between the thermal conductance of a DWCNT ($\mathrm{PTC_D}$) and the thermal conductances of the inner ($\mathrm{PTC_i}$) and outer ($\mathrm{PTC_o}$) uncoupled nanotubes forming a DWCNT. This relation is correct for temperatures less than 10–15 K. At such temperatures, the modes corresponding to the relative motion of the tubular walls are frozen. Therefore the thermal excitations in any DWCNT are fully equivalent to the modes of a SWCNT of a particular effective radius. The value of the latter is in between the radii of the inner and outer nanotubes comprising a double-walled one. Along with further temperature growth, $\mathrm{PTC_D}$ exceeds both $\mathrm{PTC_i}$ and $\mathrm{PTC_o}$ but remains lower than their sum. Thus the value of van der Waals interaction between the tubular layers determines the low-temperature thermodynamic properties of DWCNTs.

To compare our theoretical model with the available experimental data on low-temperature TC of SWCNT bundles, we use the minimal model describing the ballistic heat transfer in CNT composite materials. This model allows us to estimate the upper limits of low-temperature TC in such composites. It was found that the perfect hypothetical CNT-based composite can challenge diamond (the best-known heat conductor) only when the mean length of defect-free CNTs in the composite reaches at least one hundred of micrometers. Therefore, at present, it seems not effective to apply bulk CNT-based composite materials for the heat exchange.

ACKNOWLEDGMENTS

We gratefully acknowledge financial support of Russian Science Foundation (Grant No. 15-12-10004).

[1] A. Jorio, M. S. Dresselhaus, and G. Dresselhaus, *Carbon Nanotubes: Advanced Topics in the Synthesis, Structure, Properties and Applications* (Springer, Berlin, 2008).

[2] J. M. Marulanda, *Carbon Nanotubes Applications on Electron Devices* (InTech, 2011).
[3] J. Hone, M. Whitney, and A. Zettl, Synthetic Met. **103**, 2498 (1999).
[4] J. Hone, M. C. Llaguno, N. M. Nemes, A. T. Johnson, J. E. Fischer, D. A. Walters, M. J. Casavant, J. Schmidt, and R. E. Smalley, Appl. Phys. Lett. **77**, 666 (2000).
[5] Ch. Yu, L. Shi, Zh. Yao, D. Li, and A. Majumdar, Nano Lett. **5**, 1842 (2005).
[6] E. Pop, D. Mann, Q. Wang, K. Goodson, and H. Dai, Nano Lett. **6**, 96 (2006).
[7] M. T. Pettes and L. Shi, Adv. Funct. Mater. **19**, 3918 (2009).
[8] J. Che, T. Cagin, and W. A Goddard III, Nanotechnol. **11**, 65 (2000).
[9] S. Berber, Y.-K. Kwon, and D. Tománek, Phys. Rev. Lett. **84**, 4613 (2000).
[10] Sh. Maruyama, Physica B **323**, 193 (2002).
[11] M. Grujicic, G. Cao, and B. Gersten, Mat. Sci. Eng. B-Solid **107**, 204 (2004).
[12] K. Bi, Y. Chen, J. Yang, Y. Wang, and M. Chen, Phys. Lett. A **350**, 150 (2006).
[13] R. A. Shelly, K. Toprak, and Y. Bayazitoglu, Int. J. Heat. Mass. Tran. **53**, 5884 (2010).
[14] A. N. Imtani, J. Phys. Chem. Solids **74**, 1599 (2013).
[15] R. N. Salaway and L. V. Zhigilei, Int. J. Heat. Mass. Tran. **70**, 954 (2014).
[16] J.-W. Jiang, Carbon **81**, 688 (2015).
[17] A. V. Savin, B. Hu, and Yu. S. Kivshar, Phys. Rev. B **80**, 195423 (2009).
[18] M. A Osman and D. Srivastava, Nanotechnol. **12**, 21 (2001).
[19] S. P. Hepplestone and G. P. Srivastava, J. Phys. Conf. Ser. **92**, 012076 (2007).
[20] M. Mir, E. Ebrahimnia-Bajestan, H. Niazmand, and M. Mir, Comp. Mater. Sci. **63**, 52 (2012).
[21] Y. Gu and Y. Chen, Phys. Rev. B **76**, 134110 (2007).
[22] N. G. Mensah, G. Nkrumah, S.Y. Mensah, and F. K. A. Allotey, Phys. Lett. A **329**, 369 (2004).
[23] A. M. Marconnet, M. A. Panzer, and K. E. Goodson, Rev. Mod. Phys. **85**, 1295 (2013).
[24] N. Mingo and D. A. Broido, Phys. Rev. Lett. **95**, 096105 (2005).
[25] J. X. Cao, X. H. Yan, Y. Xiao, and J. W. Ding, Phys. Rev. B **69**, 073407 (2004).
[26] A. Khitun and K. L. Wang, Appl. Phys. Lett. **79**, 851 (2001).
[27] X. H. Yan, Y. Xiao, and Z. M. Li, J. Appl. Phys. **99**, 124305 (2006).
[28] R. Landauer, IBM J. Res. Dev. **I**, 223 (1957).
[29] R. Landauer, Philos. Mag. **21:172**, 863 (1970).
[30] T. Yamamoto, S. Konabe1, J. Shiomi, and Sh. Maruyama, Appl. Phys. Express **2**, 095003 (2009).
[31] J. Zimmermann, P. Pavone, and G. Cuniberti, Phys. Rev. B **78**, 045410 (2008).
[32] T. Yamamoto, S. Watanabe, and K. Watanabe, Phys. Rev. Lett. **92**, 075502 (2004).
[33] K. Bui, H. Nguyen, C. Cousin, A. Striolo, and D. V. Papavassiliou, J. Phys. Chem. C **116**, 4449 (2012).
[34] G. J. Hu and B. Y. Cao, Chinese Phys. B **23**, 096501 (2014).
[35] L. Cui, Y. Feng, P. Tan, and X. Zhang, Phys. Chem. Chem. Phys. **17**, 16476 (2015).
[36] X. Zhang, Phys. Lett. A **380**, 1861 (2016).
[37] Z. Ma, Z. Guo, H. Zhang, and T. Chang, AIP Adv. **7**, 065104 (2017).
[38] L. G. C. Rego and G. Kirczenow, Phys. Rev. Lett. **81**, 232 (1998).
[39] K. Schwab, E. A. Henriksen, J. M. Worlock, and M. L. Roukes, Nature (London) **404**, 974 (2000).
[40] M. J. Biercuk, M. C. Llaguno, M. Radosavljevic, J. K. Hyun, A. T. Johnson, and J. E. Fischer, Appl. Phys. Lett. **80**, 2767 (2002).
[41] F. H. Gojny, M. H. G. Wichmann, B. Fiedler, I. A. Kinloch, W. Bauhofer, A. H. Windle, and K. Schulte, Polymer **47**, 2036 (2006).
[42] A. Moisala, Q. Li, I. A. Kinloch, and A. H. Windle, Compos. Sci. Technol. **66**, 1285 (2006).
[43] R. S. Prasher, X. J. Hu, Y. Chalopin, N. Mingo, K. Lofgreen, S. Volz, F. Cleri, and P. Keblinski, Phys. Rev. Lett. **102**, 105901 (2009).
[44] A. N. Volkov and L. V. Zhigilei, Phys. Rev. Lett. **104**, 215902 (2010).
[45] A. N. Volkov and L. V. Zhigilei, Appl. Phys. Lett. **101**, 043113 (2012).
[46] S. B. Rochal, V. L. Lorman, and Yu. I. Yuzyuk, Phys. Rev. B **88**, 235435 (2013).
[47] M. V. Avramenko, I. Yu. Golushko, A. E. Myasnikova, and S. B. Rochal, Physica E **68**, 133 (2015).
[48] J. B. Pendry, J. Phys. A **16**, 2161 (1983).
[49] A. N. Cleland, *Foundations of Nanomechenics: From Solid-State Theory to Device Applications* (Springer, 2003).
[50] R. Saito, T. Takeya, T. Kimura, G. Dresselhaus, and M. S. Dresselhaus, Phys. Rev. B **57**, 4145 (1998).
[51] N. Mingo and L. Yang, Nano Lett. **8**, 3771 (2008).
[52] L. G. C. Rego and G. Kirczenow, Phys. Rev. B **59**, 13080 (1999).
[53] I. V. Krive and E. R. Mucciolo, Phys. Rev. B **60**, 1429 (1999).
[54] A. S. Volmir, *Shells in Liquid and Gas Flow* (Nauka, Moscow, 1976) [in Russian].
[55] S. S. Savinskii and V. A. Petrovskii, Phys. Solid State **44**, 1802 (2002).
[56] Sh. Zhang, M. Xia, Sh. Zhao, T. Xu, and E. Zhang, Phys. Rev. B **68**, 075415 (2003).
[57] S. P. Hepplestone, A. M. Ciavarella, C. Janke, and G. P., Surf. Sci. **600**, 3633 (2006).
[58] G. D. Mahan, Phys. Rev. B **65**, 235402 (2002).
[59] H. Suzuura and T. Ando, Phys. Rev. B **65**, 235412 (2002).
[60] L. D. Landau and E. M. Lifshitz, *Theory of Elasticity*, 3rd ed., Course of Theoretical Physics Vol. 7 (Butterworth-Heinemann, 1986).
[61] M. V. Avramenko and S. B. Rochal, Phys. Solid State **58**, 1011 (2016).
[62] D. L. Nika, E. P. Pokatilov, A. S. Askerov, and A. A. Balandin, Phys. Rev. B **79**, 155413 (2009).
[63] V. Perebeinos and J. Tersoff, Phys. Rev. B **79**, 241409(R) (2009).
[64] S. Piscanec, M. Lazzeri, J. Robertson, A. C. Ferrari, and F. Mauri, Phys. Rev. B **75**, 035427 (2007).
[65] S. Reich, C. Thomsen, and P. Ordejón, Phys. Rev. B **64**, 195416 (2001).
[66] P. B. Canham, J. Theor. Biol. **26**, 61 (1970).
[67] W. Helfrich, Z. Naturforsch C. **28**, 693 (1973).
[68] S. V. Goupalov, Phys. Rev. B **71**, 085420 (2005).
[69] K. Liu, X. Hong, M. Wu, F. Xiao, W. Wang, X. Bai, J. W. Ager, S. Aloni, A. Zettl, E. Wang, and F. Wang, Nat. Commun. **4**, 1375 (2013).

[70] M. Damnjanovic, E. Dobardzic, I. Milosevic, T. Vukovic, and B. Nikolic, New J. Phys. **5**, 148.1 (2003).
[71] G. D. Mahan and G. S. Jeon, Phys. Rev. B **70**, 075405 (2004).
[72] R. Berman, P. R. W. Hudson, and M. Martinez, J. Phys. C. **8**, 430 (1975).
[73] G. A. Slack, J. Phys. Chem. Solids **34**, 321 (1973).
[74] G. A. Slack, Phys. Rev. **127**, 694 (1962).